Supplementary Information for:

A model for the oceanic mass balance of rhenium and for the extent of Proterozoic ocean anoxia

1 Sedimentary Re concentrations in the Cariaco Basin and calculating the representative modern Re anoxic burial rate

Our modern representative Re burial rate in the anoxic sink (b_a) is derived from data from sediment core 1002B, ODP 165, in the Cariaco Basin (Table S6). The Re concentrations were measured for six 5-cm intervals ranging from a composite depth of 20 to 420 cmbsf (centimetres below seafloor), excluding measurements closer to the sediment-water interface where $[\text{Re}]_{\text{sed}}$ is markedly low (<10 ppb). The six measurements yield an average $[\text{Re}]_{\text{sed}}$ of 63.17 ppb. Based on an average gamma-ray attenuation porosity evaluator (GRAPE), wet bulk density of 1.35 g/cm^3 is calculated for core 1002B between 21 and 419 cmbsf (Peterson et al., 2000b). The corresponding dry bulk density is calculated with the following formula (Peterson et al., 2000a):

$$\text{Dry bulk density} = \frac{\text{GRAPE wet bulk density} - 1.0532}{0.4932}$$

$$= \frac{1.35 - 1.0532}{0.4932}$$

$$= 0.606\ \text{g/cm}^3$$

This is combined with an average, linear sedimentation rate of 350 m/Myr for all of site 1002 (Peterson et al., 2000b):

$$\text{Re burial rate} = [\text{Re}]_{\text{sed}} \times \text{Dry bulk density} \times \text{Linear sedimentation rate}$$

$$= 63.17\ \text{ng/g} \times 0.606\ \text{g/cm}^3 \times 0.0360\ \text{cm/yr}$$

$$= \mathbf{1.34\ ng/cm^2 \cdot yr^1}$$

Our calculated value is similar to recently published Re burial rates in anoxic sediments of the Cariaco Basin, which have a range of 1.49–1.56 ng cm^{-2} yr^{-1} (Calvert et al., 2015) and are within the uncertainty range of our data. The slight discrepancy has negligible influence on our modeling results, as verified by replicating runs with values of Calvert et al. (2015).

Table S6. Sedimentary Re Concentrations in the Cariaco Basin, ODP 165, Core 1002B.

Sample	Depth (cmbsf)	[Re] (ppb)
B1 20-25	20	64
B1 35-40	35	67
B1 115-120	115	61
B2 50-55	200	63
B2 95-100	245	54
B3 120-125	420	70

2 Statistical analysis of trends in $[Re]_{sed}$ vs. time

An inherent source of uncertainty in interpreting temporal trends from our compilation is the uneven data density through geologic time. We divided our compilation into four stages based on the temporal trends of $[Re]_{sed}$ and other redox-sensitive elements in ORM through time in combination with other paleoredox indicators (see section 5.1 in main text). To test whether the differences in $[Re]_{sed}$ of these four stages are statistically significant, we first determined from histograms that the time-binned mean $[Re]_{sed}$ in each stage do not follow a normal or log-normal distribution. Therefore, the data cannot be statistically analyzed by normal parametric methods such as a two-tailed t-test. Following the approach of Dubin and Peucker-Ehrenbrink (2015), we used bootstrap analysis to estimate the confidence interval of each of the four sets of binned time-point mean $[Re]_{sed}$. The bootstrap method is useful for estimating a data distribution when the realistic sample distribution is unknown. For every stage, random sampling of time-point mean $[Re]_{sed}$ was carried out to create 10,000 data subsets, with each subset containing a number of randomly selected values equivalent to the total number of time-point mean $[Re]_{sed}$ values in that specific stage. An important feature of bootstrap analysis is that it employs resampling with replacement, meaning that a time-point mean $[Re]_{sed}$ can be selected again even if it had been previously sampled for the same subset. For example, stage 1 contains nine time-point mean $[Re]_{sed}$ (Table S4 in the supplementary database). An example data subset sampled by the bootstrap method from this stage would be (8.4, 8.4, 11.0, 16.2, 13.3, 8.4, 19.9, 19.9, 7.4) (values in ppb). This is performed using the RANDBETWEEN function in Microsoft Excel. The mean and median of each of the 10,000 data subsets was then calculated and compiled into a histogram display. The bootstrap means follow a symmetrical normal distribution and were chosen instead of the bootstrap medians to best represent the datasets. Stage 2 was excluded from this analysis due to the low number of time-point mean $[Re]_{sed}$ values (n=3).

3 The Re sedimentary enrichment model

3.1 Construction of the Re sedimentary enrichment model

Our modeling methods follow closely those outlined in Reinhard et al. (2013), with a few adjustments as discussed below. Essentially, we relate the Re anoxic burial rate in the modern ocean, b_a, to that found in an ancient ocean with a different spatial configuration and extent of oxic, suboxic, and anoxic settings. Assuming steady-state conditions for each scenario, the two burial rates are in principle related by the size of the seawater Re reservoir, $[\mathrm{Re}]_\mathrm{M}$, which is directly controlled by the spatial extent of the three redox settings:

$$b_a{}' = b_a\left(\frac{[\mathrm{Re}]'}{[\mathrm{Re}]_\mathrm{M}}\right) \quad \text{Eq. 1}$$

$$[\mathrm{Re}]' = [\mathrm{Re}]_\mathrm{M}\left(\frac{F_{in}}{\sum A_i b_i}\right) \quad \text{Eq. 2}$$

Where $[\mathrm{Re}]'$ is the seawater Re concentration under the new steady state, F_{in} the input (riverine) flux, and $\sum A_i b_i$ the sum of output fluxes for the oxic (o), suboxic (s), and anoxic (a) sinks. Because $[\mathrm{Re}]_\mathrm{M}$ and F_{in} are assumed to be constant in our mass balance, $[\mathrm{Re}]'$ varies as a function of A_i and b_i.

$$[\mathrm{Re}]' = [\mathrm{Re}]_\mathrm{M}\left(\frac{F_{in}}{A_o b_o + A_s b_s + A_a b_a}\right)$$

By applying perturbations to this relationship in the form of increasing anoxic seafloor area, A_a, we are primarily interested in how much $[\mathrm{Re}]_{sed}$ is to be expected in anoxic sediments as larger extents of the seafloor become covered by anoxic bottom waters. (As the following derivations involve the anoxic sink only, A_a will be expressed as A for simplification.)

Offshore scaling of anoxic Re burial

A single constant value is assumed for metal burial rate in numerous previous models of marine trace metal enrichment in ORM (e.g., Scott et al., 2008; Sahoo et al., 2012; Partin et al., 2013). However, the close association of Re burial rates with the organic carbon flux to the seafloor means that, in high-productivity ocean margins, the anoxic Re burial rate is greater compared to the abyssal plain, where the organic carbon flux is lower. Applying a constant anoxic burial rate, which is mostly measured in ocean margins, to the global seafloor results in overestimation of anoxic fluxes and a model that is oversensitive to anoxic expansion. One attempt to resolve this problem is the approach of Reinhard et al. (2013), which incorporates a pseudo-spatial scaling factor that is applied to anoxic burial rates.

To construct the offshore scaling factor, we first take an algorithm expressing labile organic carbon removal to the seafloor, $B_{C_{org}}$, as a function of seawater depth, Z (Middleburg et al., 1996; 1997):

$$B_{C_{org}}(Z) = \beta e^{\alpha Z} \quad \text{Eq. 3}$$

This is then combined with global bathymetric data (Amante and Eakins, 2009) relating seawater depth to cumulative seafloor area, A:

$$B_{C_{org}}(A) = \beta e^{\alpha \cdot Z(A)} \quad \text{Eq. 4}$$

The relationship $Z(A)$ is approximated in the Reinhard et al. (2013) model by a fourth-order polynomial function, which was necessary given the small number of sampled points (n < 10). In this study, we use bathymetric data from the eTOPO database (Amante and Eakins, 2009), which has a much higher data resolution (n > 10,000) and thereby enables subsequent calculations to be performed directly for each data point without the need for a polynomial fit. The resulting relationship $B_{C_{org}}(A)$ is treated as a differentiable pseudo-function for the remainder of the calculations. Essentially, $B_{C_{org}}(A)$ dictates a hypothetical scenario where an initially authigenically neutral global seafloor becomes active with respect to organic carbon burial, starting from the shallow continental shelf and expanding into the deep ocean. As larger regions of the seafloor become authigenically active, the total C_{org} burial flux increases, although the highest local C_{org} burial rates occur in shallow waters (i.e. the first few percent of the global seafloor in our expansion scheme). To express this total flux, we integrate $B_{C_{org}}(A)$ over A:

$$F_{C_{org}}(A) = \int_0^{A'} B_{C_{org}}(A) dA \quad \text{Eq. 5}$$

where $F_{C_{org}}(A)$, the total cumulative C_{org} flux to the seafloor, is in mol per unit time. Since calculation needs to be done for each point of $B_{C_{org}}(A)$, the actual method of integration is as follows:

$$F_{C_{org}}(A_1) = \frac{1}{2}\left(B_{C_{org}}(A_0) + B_{C_{org}}(A_1)\right)(A_1 - A_0)$$
$$F_{C_{org}}(A_2) = \frac{1}{2}\left(B_{C_{org}}(A_1) + B_{C_{org}}(A_2)\right)(A_2 - A_1) + F_{C_{org}}(A_1)$$
...
$$F_{C_{org}}(A_n) = \frac{1}{2}\left(B_{C_{org}}(A_{n-1}) + B_{C_{org}}(A_n)\right)(A_{n-1} - A_n) + F_{C_{org}}(A_n)$$

The offshore-scaled, overall average local C_{org} burial rate, $\overline{b}_{C_{org}}$, is derived by dividing $F_{C_{org}}$ by A:

$$\overline{b}_{C_{org}}(A) = \frac{F_{C_{org}}(A)}{A} \qquad \text{Eq. 6}$$

$\overline{b}_{C_{org}}$ is related to the scaled Re anoxic burial rate, $\overline{b}_{Re}$, by a tunable ratio, r, which is set at a value to reproduce the modern characteristic Re anoxic burial rate (b_a; 1.34 ng cm^{-2} yr^{-1}) when $A = A_a$ (~0.11% global seafloor area):

$$\overline{b}_{Re}(A) = r \cdot \overline{b}_{C_{org}}(A) \qquad \text{Eq. 7}$$

The use of a tunable ratio removes the dependence of Re burial rate on the absolute value of $\overline{b}_{C_{org}}$, which can be extremely variable across the seafloor due to local factors such as redox fluctuations and changes in primary productivity (Reinhard et al., 2013). The resultant $\overline{b}_{Re}(A)$ curve is similar to that derived from a polynomial-approximated bathymetric profile (Fig. S1). Significantly higher Re burial rates occur during the first 10% of anoxic expansion, which is more realistic considering the predominance of high-productivity, shallow seafloor at this point in the expansion scheme. The polynomial approximation of Reinhard et al. (2013) does not account for the characteristic shoreward "hump" and underestimates Re drawdown. In sharp contrast to both curves, a metal burial rate decoupled from variable C_{org} flux results in significant overestimation of the total Re burial rate (Fig. S1).

The authigenic burial rate expected in anoxic sediments under the new steady state, B_a', is obtained by applying the ratio between the modern anoxic burial rate and the scaled anoxic burial rate, to the unscaled authigenic burial rate:

$$B_a'(A) = b_a'(A)\left[\frac{b_a}{\overline{b}_{Re}(A)}\right] \qquad \text{Eq. 8}$$

where $b_a'(A) = b_a\left[\frac{[\mathrm{Re}]'(A)}{[\mathrm{Re}]_\mathrm{M}}\right]$ by equation 1. Note that both $b_a'$and $\overline{b}_{Re}$ are dependent on A, while b_a is constant. Additionally, because $[\mathrm{Re}]' = [\mathrm{Re}]_\mathrm{M}\left(\frac{F_{in}}{\sum A_i b_i}\right)$ by equation 2, the two $[\mathrm{Re}]_\mathrm{M}$ terms cancel out, making $b_a'(A)$ independent of the size of the modern seawater Re reservoir. Authigenic sedimentary enrichment is then solved using the bulk mass accumulation rate (BMAR):

$$[\mathrm{Re}]_\mathrm{pred}(A) = \frac{B_a'(A)}{\mathrm{BMAR}} \qquad \text{Eq. 9}$$

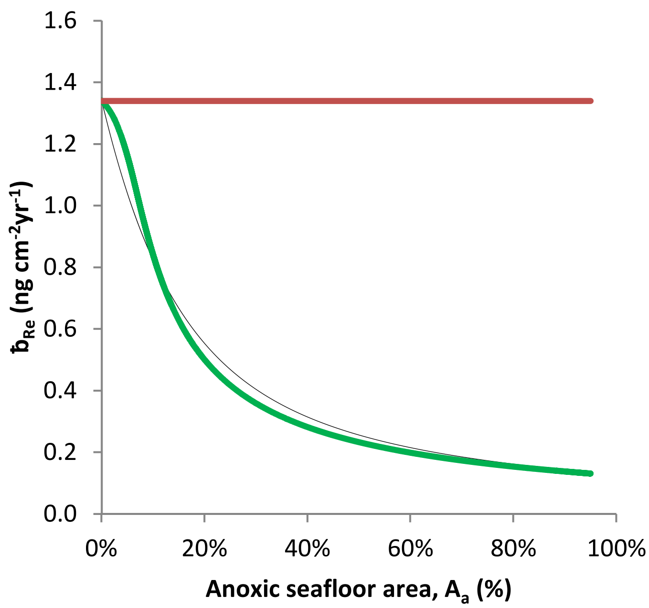

Figure S1. Tuned Re burial rate in open ocean anoxic sediments with increasing seafloor anoxia, with offshore-scaling applied (in green). Thin black curve represents the same calculations applied to a bathymetric profile derived from a fitted fourth-order polynomial function (the approach in Reinhard et al., 2013). A polynomial-fitted bathymetry results in underestimation of Re burial rate in the shallow seafloor, and slightly overestimates Re burial in the margin-proximal portion of the abyssal seafloor. In contrast, a constant anoxic burial rate applied to the entire seafloor (in red) results in significant overestimation of Re burial with expanding anoxia.

3.2 Prescribed model perturbations and treatment of the burial sinks

Anoxic expansion scheme

Our modeling analysis consists of applying perturbations to the Re mass-balance in the form of increasing anoxic seafloor and comparing the resulting $[Re]_{pred}$ in open ocean anoxic sediments with the mid-Proterozoic record. As the offshore scaling of Re burial rate introduces spatial dependence into our model, it is necessary to discuss the various assumptions we make with regards to the prescribed spatial behaviour of each redox sink. Envisioning the global ocean as a simplified bathymetric slope with the shallow continental shelf on one end and the deep ocean floor on the other, we start with a 100% oxygenated ocean and expand anoxia from the shallow shelf into the deep ocean at the expense of oxic sediments. From a mechanistic point of view, this is a reasonable approximation as modern anoxic seafloor is found in marginal settings. We set the shallowest 5% of the seafloor to be authigenically neutral. This is consistent with the assumption that atmospheric O_2 levels during the mid-Proterozoic were sufficient to maintain an oxygenated surface layer in the ocean.

Given the evidence for gas-exchange constraints as the cause for deep-ocean anoxia during the mid-Proterozoic (Canfield, 1998), one might also entertain the possibility of anoxia starting in the deep ocean and expanding shorewards. However, as we focus on constraining the lowest possible $[Re]_{pred}$ for comparison with the mid-Proterozoic $[Re]_{sed}$ record, we are primarily interested in the model trend at high extents of seafloor anoxia, upon which point the direction of expansion becomes inconsequential.

Treatment of the suboxic sink

The suboxic sink is set at a constant value independent of the prescribed perturbations, a key assumption in our modeling exercises. It is reasonable to expect that, with increasingly reducing conditions in the oceans, there will be a first-order expansion of suboxic seafloor along with anoxic seafloor. This would result in overestimating the extent of seafloor anoxia required to achieve mid-Proterozoic $[Re]_{sed}$ levels. However, from a modeling and mechanistic point of view, we believe that this is unlikely to change our basic conclusions. By fixing the magnitude of the suboxic sink at its modern average, we have already enhanced its impact in the model. More specifically, we have taken a suboxic burial rate representative of high-productivity margins and assigned it to a portion of the seafloor with maximum authigenic capacity. This slice of shallow, suboxic seafloor is set as an addition to the 100% global seafloor reserved for oxia-anoxia interaction, thereby further increasing the weight of the suboxic sink in the model via double-counting the shallow shore for both suboxia and anoxia. Furthermore, suboxia is unlikely to be a stable redox configuration at large temporal scales. Being poorly redox-buffered, fluctuations in circulation or C_{org} flux would result in the development of either true oxic or anoxic environments.

2.3 Model scenarios

Input flux variation

Low-temperature hydrothermal fluids are postulated to contribute dissolved Re to seawater, but the low-temperature hydrothermal Re input flux has not been successfully constrained. Reinhard et al. (2013) estimated that the low-temperature hydrothermal Mo flux is unlikely to exceed 10% of the Mo riverine flux. A similar approximation can be made for Re based on the generally similar geochemical characteristics of Re and Mo. To test the influence of low-temperature hydrothermal Re input to seawater, we run the model with a 110% Re input flux. Only a minor change is observed (Fig. S2).

Bathymetric variations

To simulate the expansion of epeiric seas during global sea-level high-stand, we apply inundation to 100 m and 200 m above present-day sea level in the eTOPO database. This creates a new bathymetric profile where the newly inundated land area contributes to a larger proportion of gently-sloped, shallow seafloors in the global ocean. The magnitude of prescribed sea-level rises is based on values estimated for the formation of the Ordovician and Cretaceous interior seaways (Algeo and Seslavinsky, 1995; Miller et al., 2005; Haq and Schutter, 2008). We assume that the dissolved concentration of Re remains constant during initial sea-level rise and is followed by authigenic activation of seafloor in the epeiric seas.

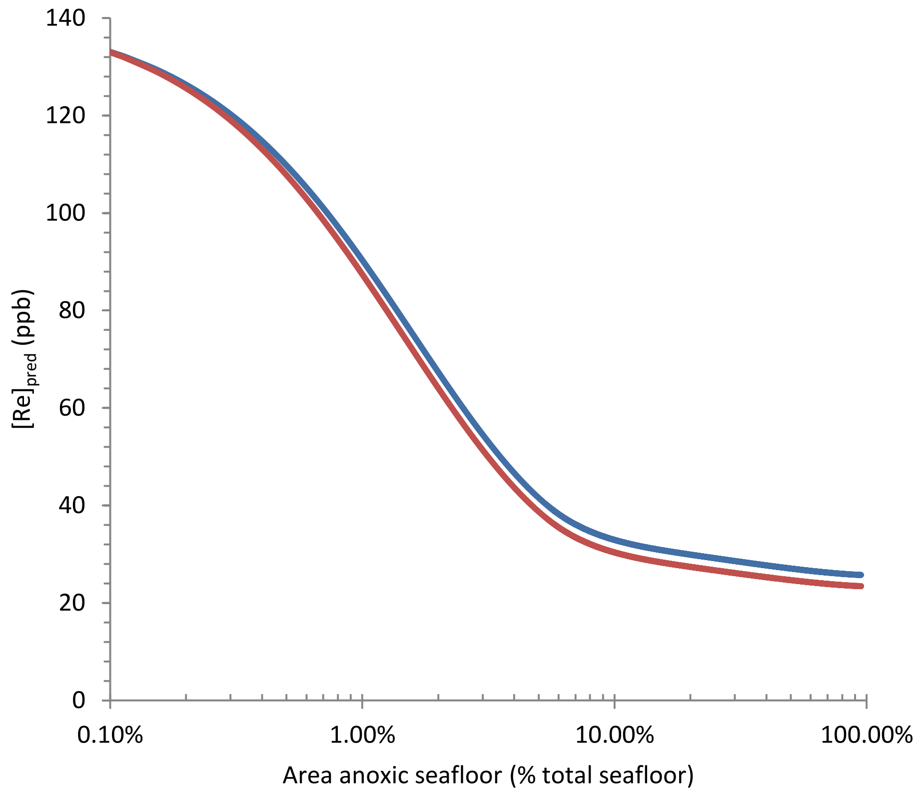

Figure S2. Modeled Re concentrations with a 10% increase in the Re input flux (in blue) compared with modeled Re concentrations with an unmodified input flux (in red). A 10% increase in the Re input flux causes a very slight increase in modeled Re concentrations.

References

Algeo T. and Seslavinsky K. (1995) Reconstructing eustatic and epeirogenic trends from Paleozoic continental flooding records. In B.U. Haq (Ed.) *Sequence Stratigraphy and Depositional Response to Eustatic, Tectonic and Climatic Forcing, Volume 1 of the series Coastal Systems and Continental Margins*, pp. 209–246.

Amante C. and Eakins B.W. (2009) ETOPO1 1 arc-minute global relief model [electronic resource]: procedures, data sources and analysis. NOAA Technical Memorandum NESDIS NGDC-24. U.S. Dept. of Commerce, National Oceanic and Atmospheric Administration, National Environmental Satellite, Data, and Information Service, National Geophysical Data Center, Marine Geology and Geophysics Division, Boulder, CO. Accessed November 20, 2014.

Calvert S. E., Piper D. Z., Thunell R. C. and Astor Y. (2015) Elemental settling and burial fluxes in the Cariaco Basin. *Mar. Chem.* **177**, 607–629.

Canfield D. E. (1998) A new model for Proterozoic ocean chemistry. *Nature* **396**, 450–453.

Haq B.U. and Schutter S.R. (2008) A chronology of Paleozoic sea-level changes. *Science* **322**, 64–68.

Middelburg J.J., Soetaert K. and Herman P.M.J. (1997) Empirical relationships for use in global diagenetic models. *Deep Sea Res. Part I* **44**, 327–344.

Middelburg J.J., Soetaert K., Herman P.M.J. and Heip C.H.R. (1996) Denitrification in marine sediments: A model study. *Global Biogeochem. Cycles* **10**, 661–673.

Miller K.G., Kominz M.A., Browning J.V., Wright J.D., Mountain G.S., Katz M.E., Sugarman P.J., Cramer B.S., Christie-Blick N. and Pekar, S.F. (2005) The Phanerozoic record of global sea-level change. *Science* **310**, 1293–1298.

Partin, C.A., Bekker, A., Planavsky, N.J., Scott, C.T., Gill, B.C., Li, C., Podkovyrov, V., Maslov, A., Konhauser, K.O., Lalonde, S.V., Love, G.D., Poulton, S.W. and Lyons, T.W. (2013) Large-scale fluctuations in Precambrian atmospheric and oceanic oxygen levels from the record of U in shales. *Earth Planet. Sci. Lett.* **369–370**, 284–293.

Peterson L.C., Haug G.H., Hughen K.A. and Röhl U. (2000a) Rapid changes in the hydrologic cycle of the tropical Atlantic during the last glacial. *Science* **290**, 1947–1951.

Peterson L.C., Haug G.H., Murray R.W., Yarincik K.M., King J.W., Bralower T.J., Kameo K., Rutherford S.D. and Pearce R.B. (2000b) Late Quaternary stratigraphy and sedimentation at Site 1002, Cariaco Basin (Venezuela). In R.M. Leckie, H. Sigurdsson, G.D. Acton and G. Draper (Eds.), *Proc. IODP* **165**, 85–99.

Reinhard C.T., Planavsky N.J., Robbins L.J., Partin C.A., Gill B.C., Lalonde S.V., Bekker A., Konhauser K.O. and Lyons T.W. (2013) Proterozoic ocean redox and biogeochemical stasis. *Proc. Natl. Acad. Sci. U.S.A.* **110**, 5357–5362.

Sahoo S.K., Planavsky N.J., Kendall B., Wang X., Shi X., Scott C., Anbar A.D., Lyons T.W. and Jiang G. (2012) Ocean oxygenation in the wake of the Marinoan glaciation. *Nature* **489**, 546–549.

Scott C., Lyons T.W., Bekker A., Shen,Y., Poulton S.W., Chu X. and Anbar A.D. (2008) Tracing the stepwise oxygenation of the Proterozoic ocean. *Nature* **452**, 456–459.

4 References for the compilation of Re in modern ORM and sediments (tables S1, S2)

Böning P., Brumsack H., Böttcher M. E., Schnetger B., Kriete C., Kallmeyer J. and Borchers S. L. (2004) Geochemistry of Peruvian near-surface sediments. *Geochim. Cosmochim. Acta.* **68**, 4429-4451.

Calvert S. E., Piper D. Z., Thunell R. C., Astor Y. (2015) Elemental settling and burial fluxes in the Cariaco Basin. *Mar. Chem.* **177**, 607-629.

Chang A. S., Pedersen T. F. and Hendy I. L. (2014) Effects of productivity, glaciation, and ventilation on late Quaternary sedimentary redox and trace element accumulation on the Vancouver Island margin, western Canada. *Paleoceanography* **29**, 730-746.

Chang A. S., Pichevin L., Pedersen T. F., Gray V. and Ganeshram R. (2015) New insights into productivity and redox-controlled trace element (Ag, Cd, Re, and Mo) accumulation in a 55 kyr long sediment record from Guaymas Basin, Gulf of California. *Paleoceangraphy* **30**, 77-94.

Colodner D., Sachs J., Ravizza G., Turekian K., Edmond J. and Boyle E. (1993) The geochemical cycle of rhenium: a reconnaissance. *Earth Planet. Sci. Lett*. **117**, 205-221.

Crusius J., Calvert S., Pedersen T. and Sage D. (1996) Rhenium and molybdenum enrichments in sediments as indicators of oxic, suboxic and sulfidic conditions of deposition. *Earth Planet. Sci. Lett.* **145**, 65-78.

Dalai T. K., Suzuki K., Minagawa M. and Nozaki Y. (2005) Variations in seawater osmium isotope composition since the last glacial maximum: A case study from the Japan Sea. *Chem. Geol.* **220**, 303-314.

Gehrke G. E., Blum J. D. and Meyers P. A. (2009) The geochemical behavior and isotopic composition of Hg in a mid-Pleistocene western Mediterranean sapropel. *Geochim. Cosmochim. Acta.* **73**, 1651-1665.

Koide M., Hodge V. F., Yang J. S., Stallard M., Goldberg E. G., Calhoun J. and Bertine K. K. (1986) Some comparative marine chemistries of rhenium, gold, silver and molybdenum. *Appl. Geochem.* **1**, 705-714.

McKay J. L., Pedersen T. F. and Mucci A. (2007) Sedimentary redox conditions in continental margin sediments (N.E. Pacific) — Influence on the accumulation of redox-sensitive trace metals. *Chem. Geol.* **238**, 180-196.

Morford J. L. and Emerson S. (1999) The geochemistry of redox sensitive trace metals in sediments. *Geochim. Cosmochim. Acta.* **63**, 1735-1750.

Morford J. L., Martin W. R. and Carney C. M. (2012) Rhenium geochemical cycling: Insights from continental margins. *Chem. Geol.* **324-325**, 73-86.

Piper D. Z. and Calvert S. E. (2011) Holocene and late glacial palaeoceanography and palaeolimnology of the Black Sea: Changing sediment provenance and basin hydrography over the past 20,000 years. *Geochim. Cosmochim. Acta.* **75**, 5597-5624.

Poirier A. (2006) Re–Os and Pb isotope systematics in reduced fjord sediments from Saanich Inlet (Western Canada). *Earth Planet. Sci. Lett.* **249**, 119-131.

Poirier A. and Hillaire-Marcel C. (2011) Improved Os-isotope stratigraphy of the Arctic Ocean. *Geophys. Res. Lett.* **38**, L14607.

Ravizza G. (1998) Osmium-isotope geochemistry of site 959: implications for Re-Os sedimentary geochronology and reconstruction of past variations in the Os-isotopic composition of seawater. In: Mascle J., Lohmann G.P. and Moullade M. (eds), *Proc. Ocean Drill. Program Part B Sci. Results.* **159**, 181-186.

Ravizza G., Turekian K. K. and Hay B. J. (1991) The geochemistry of rhenium and osmium in recent sediments from the Black Sea. *Geochim. Cosmochim. Acta.* **55**, 3741-3752.

Russell A. D. and Morford J. L. (2001) The behavior of redox-sensitive metals across a laminated–massive–laminated transition in Saanich Inlet, British Columbia. *Mar. Geol.* **174**, 341-354.

Scheiderich K., Zerkle A. L., Helz G. R., Farquhar J. and Walker R. J. (2010) Molybdenum isotope, multiple sulfur isotope, and redox-sensitive element behavior in early Pleistocene Mediterranean sapropels. *Chem. Geol.* **279**, 134-144.

van der Weijden C. H., Reichart G. and van Os B. J. H. (2006) Sedimentary trace element records over the last 200 kyr from within and below the northern Arabian Sea oxygen minimum zone. *Mar. Geol.* **231**, 69-88.

Wagner M., Hendy I. L., McKay J. L. and Pedersen T. F. (2013) Influence of biological productivity on silver and redox-sensitive trace metal accumulation in Southern Ocean surface sediments, Pacific sector. *Earth Planet. Sci. Lett.* **380**, 31-40.

Wagner M., Hendy I. L., McKay J. L. and Pedersen T. F. (2015) Redox chemistry of West Antarctic Peninsula margin surface sediments. *Chem. Geol.* **417**, 102-114.

5 References for the Re in ancient ORM compilation (tables S3, S4)

Anbar A. D., Duan Y., Lyons T. W., Arnold G. L., Kendall B., Creaser R. A., Kaufman A. J., Gordon G. W., Scott C., Garvin J. and Buick R. (2007) A Whiff of Oxygen Before the Great Oxidation Event? *Science* **317**, 1903-1906.

Arnaboldi M. and Meyers P.A. (2006) Data report: multiproxy geochemical characterization of OAE-related black shales at Site 1276, Newfoundland Basin. In Tucholke B.E., Sibuet J.-C. and Klaus A. (eds.), *Proc. Ocean Drill. Program Part B Sci. Results* **210**, 1–18.

Arnaboldi M. and Meyers P.A. (2007) Trace element indicators of increased primary production and decreased water-column ventilation during deposition of latest Pliocene sapropels at five locations across the Mediterranean Sea. *Palaeogeogr. Palaeoclimatol. Palaeoecol.* **249**, 425-443.

Baioumy H. M., Eglinton L. B. and Peucker-Ehrenbrink B. (2011) Rhenium–osmium isotope and platinum group element systematics of marine vs. non-marine organic-rich sediments and coals from Egypt. *Chem. Geol.* **285**, 70-81.

Böning P., Brumsack H., Böttcher M. E., Schnetger B., Kriete C., Kallmeyer J. and Borchers S. L. (2004) Geochemistry of Peruvian near-surface sediments. *Geochim. Cosmochim. Acta.* **68**, 4429-4451.

Bottini C., Cohen A. S., Erba E., Jenkyns H. C. and Coe A. L. (2012) Osmium-isotope evidence for volcanism, weathering, and ocean mixing during the early Aptian OAE 1a. *Geology* **40**, 583-586.

Cabral A. R., Creaser R. A., Nägler T., Lehmann B., Voegelin A. R., Belyatsky B., Pašava J., Seabra Gomes Jr. A. A., Galbiatti H., Böttcher M. E. and Escher P. (2013) Trace-element and multi-isotope geochemistry of Late-Archean black shales in the Carajás iron-ore district, Brazil. *Chem. Geol.* **362**, 91-104.

Calvert S. E., Piper D. Z., Thunell R. C. and Astor Y. (2015) Elemental settling and burial fluxes in the Cariaco Basin. *Mar. Chem.* **177**, 607-629.

Cohen A. S. (2004) The rhenium–osmium isotope system: applications to geochronological and palaeoenvironmental problems. *J. Geol. Soc. London* **161**, 729-734.

Cohen A. S. and Coe A. L. (2002) New geochemical evidence for the onset of volcanism in the Central Atlantic magmatic province and environmental change at the Triassic-Jurassic boundary. *Geology* **30**, 267-270.

Cohen A. S. Coe, A. L. Bartlett, J. M. and Hawkesworth C. J. (1999) Precise Re–Os ages of organic-rich mudrocks and the Os isotope composition of Jurassic seawater. *Earth Planet. Sci. Lett.* **167**, 159-173.

Cohen A. S., Coe A. L., Harding S. M. and Schwark L. (2004) Osmium isotope evidence for the regulation of atmospheric CO_2 by continental weathering. *Geology* **32**, 157-160.

Colodner D., Sachs J., Ravizza G., Turekian K., Edmond J. and Boyle E. (1993) The geochemical cycle of rhenium: a reconnaissance. *Earth Planet. Sci. Lett.* **117**, 205-221.

Creaser R. A., Sannigrahi P., Chacko T. and Selby D. (2002) Further evaluation of the Re-Os geochronometer in organic-rich sedimentary rocks: a test of hydrocarbon maturation effects in the Exshaw Formation, Western Canada Sedimentary Basin. *Geochim. Cosmochim. Acta* **66**, 3441-3452.

Crusius J., Calvert S., Pedersen T. and Sage D. (1996) Rhenium and molybdenum enrichments in sediments as indicators of oxic, suboxic and sulfidic conditions of deposition. *Earth Planet. Sci. Lett.* **145**, 65-78.

Dickson A. J., Cohen A. S. and Coe A. L. (2012) Seawater oxygenation during the Paleocene-Eocene Thermal Maximum. *Geology* **40**, 639-642.

Dickson A. J., Cohen A. S., Coe A. L., Davies M., Shcherbinina E. A. and Gavrilov Y. O. (2015) Evidence for weathering and volcanism during the PETM from Arctic Ocean and Peri-Tethys osmium isotope records. *Palaeogeogr. Palaeoclimatol. Palaeoecol.* **438**, 300-307.

Diekrup, D. (2011) Early Paleoproterozoic oceanic redox conditions and metabolic pathways revealed by C, S, Fe, and trace metal geochemistry. MSc thesis. Institut für Geologie und Paläontologie Westfälische Wilhelms-Universität Münster, Münster, Germany. 43 pp.

Du Vivier A. D. C. (2014) Global evaluation of Os and Ca marine isotope stratigraphy and U-Pb geochronology of the OAE 2. Ph. D. thesis. Durham University, Durham, UK. 241 pp.

Du Vivier A. D. C., Selby D., Sageman B. B., Jarvis I., Gröcke D. R. and Voigt S. (2014) Marine $^{187}Os/^{188}Os$ isotope stratigraphy reveals the interaction of volcanism and ocean circulation during Oceanic Anoxic Event 2. *Earth Planet. Sci. Lett.* **389**, 23-33.

Dubin A. and Peucker-Ehrenbrink B. (2015) The importance of organic-rich shales to the geochemical cycles of rhenium and osmium. *Chem. Geol.* **403**, 111–120.

Dumoulin J.A., Slack J.F., Whalen M.T. and Harris A.G. (2011) Depositional setting and geochemistry of phosphorites and metalliferous black shales in the Carboniferous–Permian Lisburne Group, northern Alaska. USGS Professional Paper **1776-C**, 64 pp.

Finlay A. J. (2015) Re–Os and PGE geochemistry of organic-rich sedimentary rocks and petroleum. Ph. D. thesis. Durham University, Durham, UK. 125 pp.

Finlay A. J., Selby D. and Gröcke D. R. (2010) Tracking the Hirnantian glaciation using Os isotopes. *Earth Planet. Sci. Lett.* **293**, 339-348.

Fu Y., Dong L., Li C., Qu W., Pei H., Qiao W. and Shen B. (2016) New Re–Os isotopic constrains on the formation of the metalliferous deposits of the Lower Cambrian Niutitang Formation. *J. Earth Sci.* **27**, 2.

Fu X., Wang J., Qu W., Duan T., Du A., Wang Z. and Liu H. (2008). Re–Os (ICP-MS) dating of marine oil shale in the Qiangtang Basin, northern Tibet, China. *Oil Shale* **25**, 44-55.

Geboy N.J., Tripaty G.R., Ruppert L.F., Eble C.F., Blake B.M., Hannah J.L. and Stein H.J. (2015) Re–Os age for the Lower-Middle Pennsylvanian Boundary and comparison with associated palynoflora. *Int. J. Coal Geol.* **140**, 23-30.

Georgiev S., Stein H. J., Hannah J. L., Bingen B., Weiss H. M. and Piasecki S. (2011) Hot acidic Late Permian seas stifle life in record time. *Earth Planet. Sci. Lett.* **310**, 389-400.

Georgiev S., Stein H. J., Hannah J. L., Weiss H. M., Bingen B., Xu G., Rein E., Hatlö V., Löseth H., Nali M. and Piasecki S. (2012) Chemical signals for oxidative weathering predict Re–Os isochroneity in black shales, East Greenland. *Chem. Geol.* **324-325**, 108-121.

Georgiev S., Stein H. J., Hannah J. L., Henderson C. M. and Algeo T. J. (2015) Enhanced recycling of organic matter and Os-isotopic evidence for multiple magmatic or meteoritic inputs to the Late Permian Panthalassic Ocean, Opal Creek, Canada. *Geochim. Cosmochim. Acta* **150**, 192-210.

Georgiev S.V., Stein H.J., Hannah J.L., Xu G., Bingen B. and Weiss H.M. (2017) Timing, duration, and causes for Late Jurassic-Early Cretaceous anoxia in the Barents Sea. *Earth Planet. Sci. Lett*. **461**, 151-162.

Gibson T. M., Cumming V. M., Creaser R. A., Wörndle S., Hodgskiss M. and Halverson G. P. (2016) New Re–Os geochronological constraints on the evolution of the Bylot Supergroup in the Borden Basin, Baffin Island. *GAC-MAC Joint Annual Meeting, Program with Abstracts*, p.39.

Gordon G. W., Rockman M., Turekian K. K. and Over J. (2009) Osmium isotopic evidence against an impact at the Frasnian-Famennian boundary. *Am. J. Sci.* **309**, 420-430.

Harris N. B., Mnich C. A., Selby D. and Korn D. (2013) Minor and trace element and Re–Os chemistry of the Upper Devonian Woodford Shale, Permian Basin, west Texas: Insights into metal abundance and basin processes. *Chem. Geol.* **356**, 76-93.

Horan M. F., Morgan J. W., Grauch R. I., Coveney Jr. R. M., Murowchick J. B. and Hulbert L. J. (1994) Rhenium and osmium isotopes in black shales and Ni-Mo-PGE-rich sulfide layers, Yukon Territory, Canada, and Hunan and Guizhou provinces, China. *Geochim. Cosmochim. Acta* **58**, 257-265.

Jaffe L. A., Peucker-Ehrenbrink B. and Petsch S. T. (2002) Mobility of rhenium, platinum group elements and organic carbon during black shale weathering. *Earth Planet. Sci. Lett.* **198**, 339-353.

Jiang S., Yang J., Ling H., Chen Y., Feng H., Zhao K. And Ni P. (2007) Extreme enrichment of polymetallic Ni–Mo–PGE–Au in Lower Cambrian black shales of South China: An Os isotope and PGE geochemical investigation. *Palaeogeogr. Palaeoclimatol. Palaeoecol.* **254**, 217-228.

Kendall B., Creaser R. A., Ross G. M. and Selby D. (2004) Constraints on the timing of Marinoan "Snowball Earth" glaciation by ^{187}Re–^{187}Os dating of a Neoproterozoic, post-glacial black shale in Western Canada. *Earth Planet. Sci. Lett.* **222**, 729-740.

Kendall B., Creaser R. A. and Selby D. (2006) Re-Os geochronology of postglacial black shales in Australia: Constraints on the timing of “Sturtian” glaciation. *Geology* **34**, 729-732.

Kendall B., Creaser R. A., Calver C. R., Raub T. D. and Evans D. A. D. (2009a) Correlation of Sturtian diamictite successions in southern Australia and northwestern Tasmania by Re–Os black shale geochronology and the ambiguity of "Sturtian"-type diamictite–cap carbonate pairs as chronostratigraphic marker horizons. *Precambrian Res.* **172**, 301-310.

Kendall B., Creaser R. A., Gordon G. W. and Anbar A. D. (2009b) Re–Os and Mo isotope systematics of black shales from the Middle Proterozoic Velkerri and Wollogorang Formations, McArthur Basin, northern Australia. *Geochim. Cosmochim. Acta* **73**, 2534-2558.

Kendall B., Creaser R. A. and Selby D. (2009c) ^{187}Re-^{187}Os geochronology of Precambrian organic-rich sedimentary rocks. *Geol. Soc. London Spec. Publ.* **326**, 85-107.

Kendall B., Reinhard C. T., Lyons T. W., Kaufman A. J., Poulton S. W. and Anbar A. D. (2010) Pervasive oxygenation along late Archaean ocean margins. *Nat. Geosci*. **3**, 647-652.

Kendall B., van Acken D. and Creaser R. A. (2013) Depositional age of the early Paleoproterozoic Klipputs Member, Nelani Formation (Ghaap Group, Transvaal Supergroup, South Africa) and implications for low-level Re–Os geochronology and Paleoproterozoic global correlations. *Precambrian Res.* **237**, 1-12.

Kendall B., Creaser R. A., Reinhard C. T., Lyons T. W. and Anbar A. D. (2015) Transient episodes of mild environmental oxygenation and oxidative continental weathering during the late Archean. Sci. Adv. **1**, e1500777.

Koide M., Hodge V. F., Yang J. S., Stallard M., Goldberg E. G., Calhoun J. and Bertine K. K. (1986) Some comparative marine chemistries of rhenium, gold, silver and molybdenum. *Appl. Geochem.* **1**, 705-714.

Lu X., Kendall B., Stein H.J., Li C., Hannah J.L., Gordon G.W. and Ebbestad J.O.R. (2017) Marine redox conditions during deposition of Late Ordovician and Early Silurian organic-rich mudtocks in the Siljan ring district, central Sweden. *Chem. Geol.* **457**, 75-94.

Manikyamba C. and Kerrich R. (2006) Geochemistry of black shales from the Neoarchaean Sandur Superterrane, India: First cycle volcanogenic sedimentary rocks in an intraoceanic arc-trench complex. *Geochim. Cosmochim. Acta* **70**, 4663-4679.

Markey R., Stein H.J., Hannah J.L., Georgiev S.V., Pedersen J.H. and Dons C.E. (2017) Re–Os identification of glide faulting and precise ages for correlation from the Upper Jurassic Hekkingden Formation, southwestern Barents Sea. *Palaeogeogr. Palaeoclimatol. Palaeoecol.* **466**, 209-220.

März C., Vogt C., Schnetger B. And Brumsack H. (2011) Variable Eocene-Miocene sedimentation processes and bottom water redox conditions in the Central Arctic Ocean (IODP Expedition 302). *Earth Planet. Sci. Lett.* **310**, 526-537.

Pašava J., Oszczepalski S. and Du A. (2010) Re–Os age of non-mineralized black shale from the Kupferschiefer, Poland, and implications for metal enrichment. *Miner. Deposita.* **45,** 189-199.

Pearce C. R., Cohen A. S., Coe A. L., Burton K. W. (2008) Molybdenum isotope evidence for global ocean anoxia coupled with perturbations to the carbon cycle during the Early Jurassic. *Geology* **36**, 231-234.

Pearce C. R., Coe A. L. and Cohen A. S. (2010) Seawater redox variations during the deposition of the Kimmeridge Clay Formation, United Kingdom (Upper Jurassic): Evidence from molybdenum isotopes and trace metal ratios. *Paleoceanography* **25**, 15 pp.

Peucker-Ehrenbrink B. and Hannigan R. E. (2000) Effects of black shale weathering on the mobility of rhenium and platinum group elements. *Geology* **28**, 475-478.

Pitcher L. L. (2013) The Upper Pennsylvanian Hushpuckney 'Core' Black Shale Member from the Swope Formation in Kansas: Rhenium - Osmium Isotope Systematics, and the Highly Siderophile Elements. M. Sc. thesis. Stony Brook University, Stony Brook, NY. 48 pp.

Poirier A. (2006) Re–Os and Pb isotope systematics in reduced fjord sediments from Saanich Inlet (Western Canada). *Earth Planet. Sci. Lett.* **249**, 119-131.

Poirier A. and Hillaire-Marcel C. (2011) Improved Os-isotope stratigraphy of the Arctic Ocean. Geophys. Res. Lett. **38**, 6 pp.

Porter S. J. (2012) Nickel and osmium isotope and trace element geochemistry of organic-rich sedimentary rocks: The first investigation of Ni isotope systematics in marine sediments. Ph. D. thesis. Durham University, Durham, UK. 235 pp.

Porter S. J., Selby D., Suzuki K. and Gröcke D. R. (2013) Opening of a trans-Pangaean marine corridor during the Early Jurassic: Insights from osmium isotopes across the Sinemurian-Pliensbachian GSSP, Robin Hood's Bay, UK. *Palaeogeogr. Palaeoclimatol. Palaeoecol.* **375**, 50-58.

Porter S. J., Smith P. L., Caruthers A. H., Hou P., Gröcke D. R. and Selby D. (2014) New high resolution geochemistry of Lower Jurassic marine sections in western North America: A global positive carbon isotope excursion in the Sinemurian? *Earth Planet. Sci. Lett.* **397**, 19-31.

Ravizza G. (1998) Osmium-isotope geochemistry of Site 959: implications for Re-Os sedimentary geochronology and reconstruction of past variations in the Os-isotopic composition of seawater. *Proc. ODP, Sci. Results.* **159**, 177-184.

Ravizza G. and Paquay F. (2008) Os isotope chemostratigraphy applied to organic-rich marine sediments from the Eocene-Oligocene transition on the West African margin (ODP Site 959). *Paleoceanography* **23**, 11 pp.

Ravizza G. and Turekian K. K. (1989) Application of the ^{187}Re-^{187}Os system to black shale geochronometry. *Geochim. Cosmochim. Acta* **53**, 3257-3262.

Rooney A. D., Selby D., Houzay J. and Renne P. R. (2010) Re–Os geochronology of a Mesoproterozoic sedimentary succession, Taoudeni basin, Mauritania: Implications for basin-wide correlations and Re–Os organic-rich sediments systematics. *Earth Planet. Sci. Lett.* **289**, 486-496.

Rooney A. D., Chew D. M. and Selby D. (2011) Re–Os geochronology of the Neoproterozoic-Cambrian Dalradian Supergroup of Scotland and Ireland: Implications for Neoproterozoic stratigraphy, glaciations and Re–Os systematics. *Precambrian Res.* **185**, 202-214.

Rooney A. D., Strauss J. V., Brandon A. D. and Macdonald F. A. (2015) A Cryogenian chronology: Two long-lasting synchronous Neoproterozoic glaciations. *Geology* **43**, 459-462.

Ross D. J. K. and Bustin R. M. (2009) Investigating the use of sedimentary geochemical proxies for paleoenvironment interpretation of thermally mature organic-rich strata: Examples from the Devonian–Mississippian shales, Western Canadian Sedimentary Basin. *Chem. Geol.* **260**, 1-19.

Russell A. D. and Morford J. L. (2001) The behavior of redox-sensitive metals across a laminated–massive–laminated transition in Saanich Inlet, British Columbia. *Mar. Geol.* **174**, 341-354.

Schaefer B. F. and Burgess J. M. (2003) Re–Os isotopic age constraints on deposition in the Neoproterozoic Amadeus Basin: implications for the 'Snowball Earth'. *J. Geol. Soc. London* **160**, 825-828.

Schoepfer S. D., Henderson C. M., Garrison G. H., Foriel J., Ward P. D., Selby D., Hower J. C., Algeo T. J. and Shen Y. (2013) Termination of a continent-margin upwelling system at the Permian–Triassic boundary (Opal Creek, Alberta, Canada). *Global and Planet. Change; New Developments in Permian-Triassic Paleoceanographic and Global Climate System Research* **105**, 21-35.

Scott C., Lyons T.W., Bekker A., Shen Y., Poulton S.W., Chu X. and Anbar A.D. (2008) Tracing the stepwise oxygenation of the Proterozoic ocean. *Nature* **452**, 456–459.

Selby D. (2007) Direct Rhenium-Osmium age of the Oxfordian-Kimmeridgian boundary, Staffin bay, Isle of Skye, U.K., and the Late Jurassic time scale. *Norw. J. Geol.* **87**, 291-299.

Selby D. and Creaser R. A. (2003) Re–Os geochronology of organic rich sediments: an evaluation of organic matter analysis methods. *Chem. Geol.* **200**, 225-240.

Selby D. and Creaser R. A. (2005) Direct radiometric dating of the Devonian-Mississippian time-scale boundary using the Re-Os black shale geochronometer. *Geology* **33**, 545-548.

Selby D., Mutterlose J. and Condon D. J. (2009) U–Pb and Re–Os geochronology of the Aptian/Albian and Cenomanian/Turonian stage boundaries: Implications for timescale calibration, osmium isotope seawater composition and Re–Os systematics in organic-rich sediments. *Chem. Geol.* **265**, 394-409.

Siebert C., Kramers J. D., Meisel T., Morel P. and Nägler T. F. (2005) PGE, Re-Os, and Mo isotope systematics in Archean and early Proterozoic sedimentary systems as proxies for redox conditions of the early Earth. *Geochim. Cosmochim. Acta* **69**, 1787-1801.

Singh S. K., Trivedi J. R. and Krishnaswami S. (1999) Re-Os isotope systematics in black shales from the Lesser Himalaya: their chronology and role in the $^{187}Os/^{188}Os$ evolution of seawater. *Geochim. Cosmochim. Acta* **63**, 2381-2392.

Strauss J. V., Rooney A. D., Macdonald F. A., Brandon A. D. and Knoll A. H. (2014) 740 Ma vase-shaped microfossils from Yukon, Canada: Implications for Neoproterozoic chronology and biostratigraphy. *Geology* **42**, 659-662.

Tejada M. L. G., Suzuki K., Kuroda J., Coccioni R., Mahoney J. J., Ohkouchi N., Sakamoto T. and Tatsumi, Y. (2009) Ontong Java Plateau eruption as a trigger for the early Aptian oceanic anoxic event. *Geology* **37**, 855-858.

Tripathy G.R. and Singh S.K. (2015) Re-Os depositional age for black shales from the Kaimur Group, Upper Vindhyan, India. *Chem. Geol.* **413**, 63-72.

Tripathy G. R., Hannah J. L., Stein H. J. and Yang G. (2014) Re-Os age and depositional environment for black shales from the Cambrian-Ordovician boundary, Green Point, western Newfoundland. *Geochem. Geophys. Geosyst*. **15**, 1021-1037.

Turgeon S. C. and Creaser R. A., 2008. Cretaceous oceanic anoxic event 2 triggered by a massive magmatic episode. *Nature* **454**, 323-326.

Turgeon S. C., Creaser R. A. and Algeo T. J. (2007) Re–Os depositional ages and seawater Os estimates for the Frasnian–Famennian boundary: Implications for weathering rates, land plant evolution, and extinction mechanisms. *Earth Planet. Sci. Lett.* **261**, 649-661.

van Acken D., Thomson D., Rainbird R. H. and Creaser R. A. (2013) Constraining the depositional history of the Neoproterozoic Shaler Supergroup, Amundsen Basin, NW Canada: Rhenium-osmium dating of black shales from the Wynniatt and Boot Inlet Formations. *Precambrian Res.* **236**, 124-131.

Wieczorek R., Fantle M. S., Kump L. R. and Ravizza G. (2013) Geochemical evidence for volcanic activity prior to and enhanced terrestrial weathering during the Paleocene Eocene Thermal Maximum. *Geochim. Cosmochim. Acta* **119**, 391-410.

Wille M., Kramers J. D., Nägler T. F., Beukes N. J., Schröder S., Meisel T., Lacassie J. P. and Voegelin A. R., 2007. Evidence for a gradual rise of oxygen between 2.6 and 2.5 Ga from Mo isotopes and Re-PGE signatures in shales. *Geochim. Cosmochim. Acta* **71**, 2417-2435.

Xiang L., Cai C., He X., Jiang L., Yuan Y., Wang T., Jia L. and Yu L. (2016) The Ocean Redox State Evolution and Its Controls during the Cambrian Series 1–2: Evidence from Lijiatuo Section, South China. *J. Earth Sci.* **27**, 255-270.

Xu G., Hannah J. L., Stein H. J., Bingen B., Yang G., Zimmerman A., Weitschat W., Mørk A. and Weiss H. M. (2009) Re–Os geochronology of Arctic black shales to evaluate the Anisian–Ladinian boundary and global faunal correlations. *Earth Planet. Sci. Lett.* **288**, 581-587.

Xu G., Hannah J. L., Bingen B., Georgiev S. and Stein H. J. (2012) Digestion methods for trace element measurements in shales: Paleoredox proxies examined. *Chem. Geol.; Special Issue Recent Advances in Trace Metal Applications to Paleoceanographic Studies* **324-325**, 132-147.

Xu,G., Hannah J. L., Stein H. J., Mørk A., Vigran J. O., Bingen B., Schutt D. L. and Lundschien B. A. (2014) Cause of Upper Triassic climate crisis revealed by Re–Os geochemistry of Boreal black shales. *Palaeogeogr. Palaeoclimatol. Palaeoecol.* **395**, 222-232.

Yang G., Hannah J. L., Zimmerman A., Stein H. J., Bekker A. (2009) Re–Os depositional age for Archean carbonaceous slates from the southwestern Superior Province: Challenges and insights. *Earth Planet. Sci. Lett.* **280**, 83-92.

Zhu B., Becker H., Jiang S., Pi D., Fischer-Gödde M. and Yang J. (2013) Re–Os geochronology of black shales from the Neoproterozoic Doushantuo Formation, Yangtze platform, South China. *Precambrian Res.; Biogeochemical Changes Across the Ediacaran-Cambrian Transition in South China* **225**, 67-76.